PROCEEDINGS OF SPIE

SPIEDigitalLibrary.org/conference-proceedings-of-spie

Towards nonionizing photoacoustic cystography

Chulhong Kim, Mansik Jeon, Lihong V. Wang

Chulhong Kim, Mansik Jeon, Lihong V. Wang, "Towards nonionizing photoacoustic cystography," Proc. SPIE 8223, Photons Plus Ultrasound: Imaging and Sensing 2012, 82231U (23 February 2012); doi: 10.1117/12.905793

SPIE.

Event: SPIE BiOS, 2012, San Francisco, California, United States

Towards Nonionizing Photoacoustic Cystography

Chulhong Kim[1*], Mansik Jeon[1], and Lihong V. Wang[2]

[1]Department of Biomedical Engineering, University at Buffalo, The State University of New York, Buffalo, New York 12260
[2]Department of Biomedical Engineering, Washington University in St. Louis, Campus Box 1097, One Brookings Dr. St. Louis, Missouri, 63130

*Corresponding author: Chulhong@buffalo.edu

ABSTRACT

Normally, urine flows down from kidneys to bladders. Vesicoureteral reflux (VUR) is the abnormal flow of urine from bladders back to kidneys. VUR commonly follows urinary tract infection and leads to renal infection. Fluoroscopic voiding cystourethrography and direct radionuclide voiding cystography have been clinical gold standards for VUR imaging, but these methods are ionizing. Here, we demonstrate the feasibility of a novel and nonionizing process for VUR mapping in vivo, called photoacoustic cystography (PAC). Using a photoacoustic (PA) imaging system, we have successfully imaged a rat bladder filled with clinically being used methylene blue dye. An image contrast of ~8 was achieved. Further, spectroscopic PAC confirmed the accumulation of methylene blue in the bladder. Using a laser pulse energy of less than 1 mJ/cm^2, bladder was clearly visible in the PA image. Our results suggest that this technology would be a useful clinical tool, allowing clinicians to identify bladder noninvasively *in vivo*.

Keywords: Photoacoustic tomography, nonionizing, bladder imaging, methylene blue.

INTRODUCTION

Vesicoureteral reflux (VUR), the retrograde flow of urine from the bladder into the upper urinary tract, is commonly diagnosed after patients (typically children) have a urinary tract infection. [1-3] By transporting bacteria from the bladder back to the upper urinary tract, VUR causes renal infections such as pyelonephritis. The immunological and inflammatory reaction due to the renal infection may cause renal injury or scarring. Severe renal scarring may reduce renal function and produce severe side effects, including renal insufficiency, endstage renal disease, renin-mediated hypertension, decreased somatic growth, and morbidity during pregnancy. Early detection and treatment of VUR is essential. Two main methods have been used to evaluate VUR: fluoroscopic voiding cystourethrography (VCUG) and direct radionuclide voiding cystography (DRNC) [2]. Although radiation dose reduction has been achieved in fluoroscopic VCUG, this method is still ionizing. Further, despite the smaller radiation dose of DRNC, this technique suffers from low spatial resolution, and patients are still exposed to radiation. The pediatric VUR guidelines panel of the American Urological Association strongly urges the development of techniques with less radiation exposure. [1,3] Echo-enhanced urosonography has been recently applied to monitor VUR, and it offers the advantages of nonionizing, real-time, and portable imaging capability. [2] However, ultrasound (US) imaging suffers from low image contrast because of speckle artifacts. Therefore, US imaging alone cannot be used for VUR tracking.

Photoacoustic (PA) imaging is a non-ionizing and noninvasive imaging technique that can supply strong optical absorption contrast with high ultrasonic spatial resolution. [4] In PA imaging, a short-pulsed laser is used to irradiate the tissue, and the PA waves excited via thermoelastic expansion. The generated PA waves propagate in the medium and are then detected by an ultrasonic transducer. The acquired PA data based on the arrival times of the acoustic waves are used to quantify the optical absorption distribution. PA image contrast is determined by optical absorption in the PA excitation phase, whereas its resolution is mainly derived from ultrasonic detection in the PA emission phase. Most importantly, the PA amplitudes are directly proportional to optical absorption coefficients of targets, which are strongly related to oxygen saturation and total concentration of hemoglobin. Recently, PAT has been extensively explored in preclinical and clinical studies, including primary cancer detection, lymph node staging and

Photons Plus Ultrasound: Imaging and Sensing 2012, edited by Alexander A. Oraevsky, Lihong V. Wang,
Proc. of SPIE Vol. 8223, 82231U · © 2012 SPIE · CCC code: 1605-7422/12/$18 · doi: 10.1117/12.905793

lymphangiography, brain activation, ophthalmology, image-guided therapy, etc. [5-9] A clinical ultrasonic scanner has been adapted to PAT, combining the high contrast of optical imaging and the high resolution of ultrasound imaging. [10-13]

In this proceedings, for the first time to our knowledge, we describe the feasibility of a novel and safe approach for VUR monitoring using PAT, referred to as photoacoustic cystography (PAC). As the first step, a healthy rat bladder filled with methylene blue was photoacoustically imaged *in vivo* without any ionizing radiation.

METHODS AND MATERIALS

A photograph of a dark-field confocal photoacoustic imaging system [14] is shown in Figure 1. A tunable OPO laser (400 - 2300 nm, Surelite III OPO, Continuum), pumped by a Q-switched Nd:YAG laser with 6-ns pulse duration and 10-Hz pulse repetition rate, is used as a light source. A light wavelength of 667 nm was used for most of the experiments, but both 667 and 850 nm optical wavelengths were used for spectroscopic bladder identification. Formed by a spherical conical lens and an optical condenser, the donut-shaped light illumination was coaxially aligned with the ultrasound focus in water. Dark-field confocal configuration provided a greater penetration depth and higher SNR. The light fluences on the skin were less than 1 mJ/cm^2, within the ANSI limit. A 5-MHz single-element ultrasound transducer was used as a detector. The axial and transverse resolutions are 144 μm and 590 μm, respectively. The scanning speed for one PA image was ~ 25 minutes, with a field of view (FOV) of 2.5 × 2.5 cm in x and y axes, respectively. No signal was averaged. By measuring PA amplitudes according to their arrival times, one-dimensional depth-resolved image could be acquired, referred to as an A-line. Additional raster scanning along the one transverse direction enables the formation of two-dimensional depth-resolved images (B-scans). The acquired two-dimensional raw data can be processed: a maximum amplitude projection (MAP), a projection of the maximum PA amplitude along each A-line onto the corresponding plane.

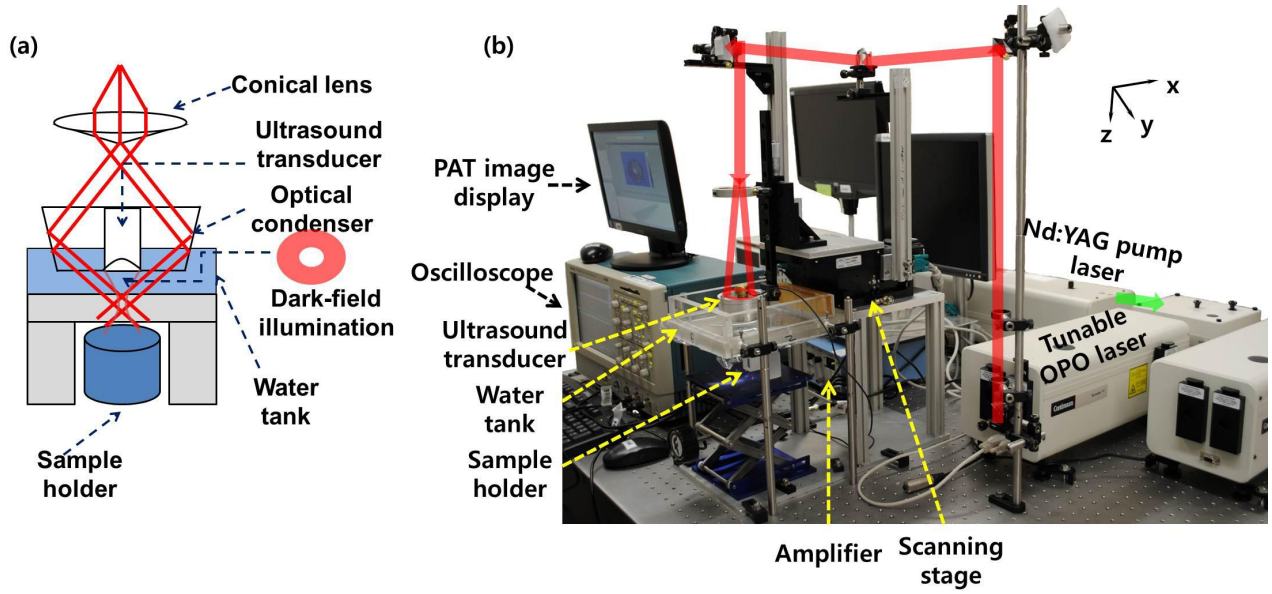

Figure 1: Schematic and photograph of volumetric photoacoustic imaging system. (a) Schematic of the dark-field light illuminaton PA system. (b) Photograph of the PA system. OPO laser; Optical parametric oscillator laser.

Spraque-Dawley rats weighing about 250 g were used for the *in-vivo* experiments. All *in vivo* animal experiments were carried out in compliance with the Institutional Animal Care and Use Committee. The rats were initially anesthetized with a mixture of ketamine (85 mg/kg) and xylazine (15 mg/kg). After depilation in the abdominal region, the rats were positioned atop a home-made holder (Figure 2a). The distal end of a 22 gauge catheter was coated with lubricant. After the urinary meatus was identified, the catheter was gently inserted until urine was noted. Then, urine in the bladder was allowed to void through the catheter. Before injection of dye, we obtained a control image. Figure 2b is a photograph of a rat taken prior to PA image acquisition and after hair removal and catheterization. After

injection of methylene blue, with a concentration of 30 mM and a dose of 0.2 ml via the catheter, we acquired a series of PA images. Figure 2c shows a photograph of the same region with skin removed and shows the bladder containing methylene blue after the PA imaging.

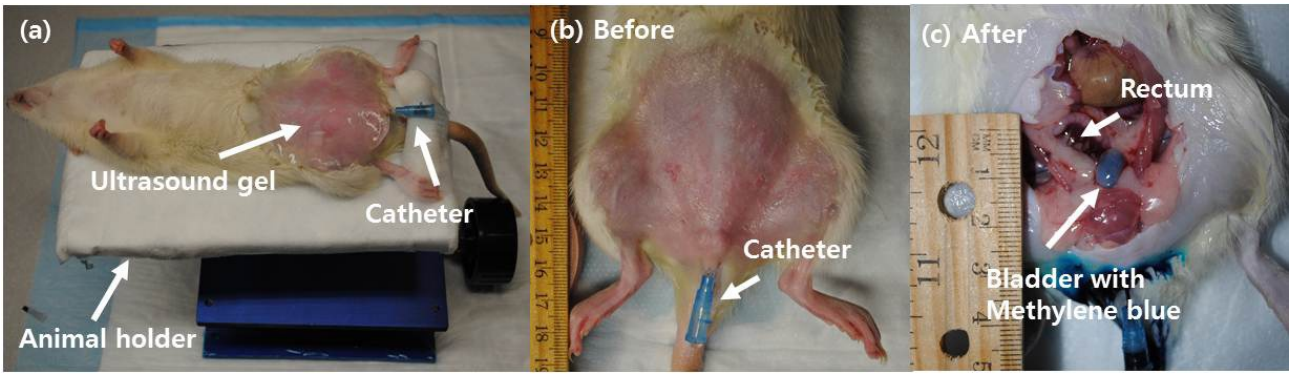

Figure 2: (a) Photography of an animal with bladder catherization and animal holder. (b) Photograph with hair removed before photoacoustic imaging. (c) Photography with skin removed after photoacoustic imaging.

RESULTS AND DISCUSSIONS

The pre-injection control PA image was obtained at a wavelength of 667 nm, where the optical absorption of methylene blue is peak, and is shown in the form of maximum amplitude projection (MAP) in Figure 3a. The vasculature in the abdominal area was clearly imaged with high contrast. The bladder was not visible in the control PA image because urine in the bladder was optically transparent at the 667 nm wavelength. The bladder appeared clearly in the PA image acquired after methylene blue injection. Because methylene blue has higher optical absorption than blood at the 667 nm wavelength, the bladder appeared with a much higher contrast than the surrounding blood vessels (Figure 3b).

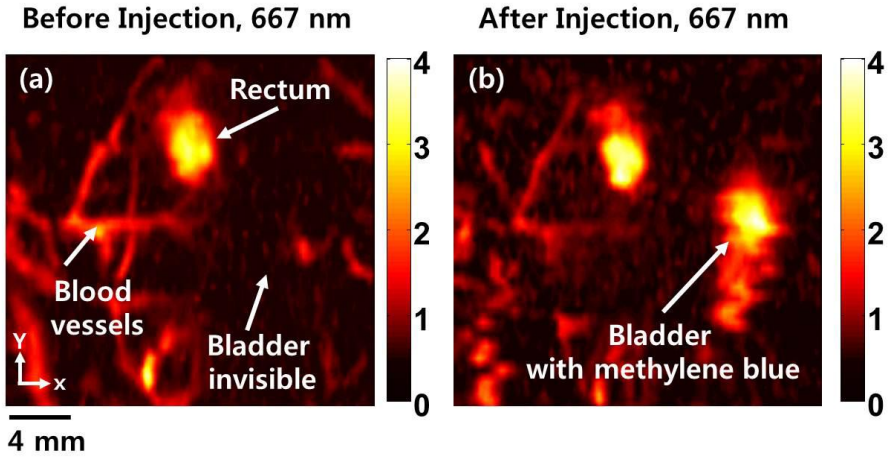

Figure 3: *In vivo* nonionizing and noninvasive PA bladder imaging in a rat using methylene blue injection. (a) Control PA image at 667 nm without methylene blue. (b) PA image acquired at 667 nm after injection.

The bladder filled with methylene blue is also clearly mapped in the depth-resolved PA B-scan image (Figure 3). The bladder was positioned ~ 2 mm below the skin surface. Again, the bladder was invisible in the control PA B-scan image (Figure 4a). The accumulation of methylene blue in the bladder was visually identified in a photograph of the same rat with the skin removed after PA imaging (Figure 4b).

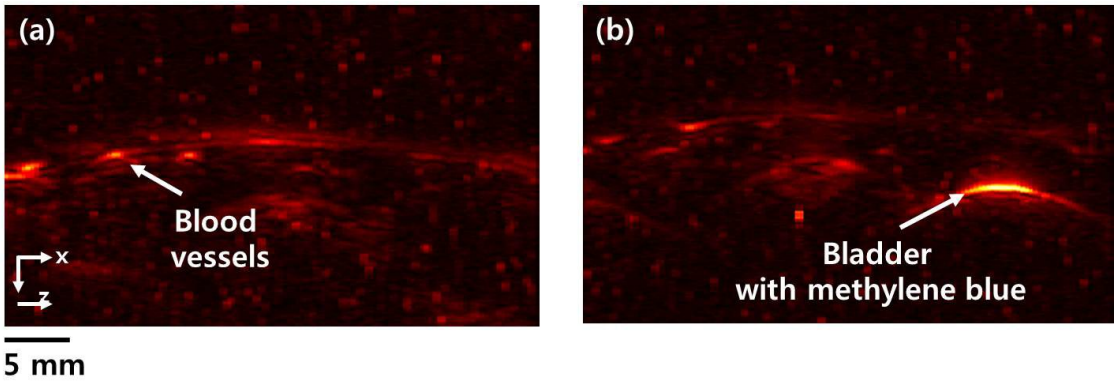

Figure4: B-scan PA images of bladder before and after injection of methylene blue. (a) Control B-scan PA image. (b) B-scan PA image after injection.

CONCLUSIONS

In summary, we have shown the feasibility of a new and safe imaging method for tracking VUR. Conventional imaging techniques suffer from either ionizing radiation or low image contrast. For the first step, photoacoustically and spectrally imaged a rat bladder filled with clinically used methylene blue dye in vivo. The nonionizing PAC can completely avoid radiation exposure to child subjects. Once it is combined with a conventional US imaging probe, this technique can be portable, fast, and cost effective. In the future, we will investigate the PA VUR mapping in a porcine model. In addition, PAC can be potentially used for other urologic diseases such as bladder cancers. Once it is combined with a conventional US imaging probe, this technique can be portable, fast, and cost effective. In the future, we will investigate the PA VUR mapping in a porcine model. In addition, PAC can be potentially used for other urologic diseases such as bladder cancers.

ACKNOWLEDGEMENT

This work was supported in part by the University at Buffalo Research Foundation faculty start-up fund. We thank Drs. Saul Greenfield and Wayne Waz for fruitful scientific discussions.

REFERENCES

[1] J. S. Elder, et al., “Pediatric Vesicoureteral Reflux Guidelines Panel Summary Report On The Management Of Primary Vesicoureteral Reflux In Children,” J. Urol. **157**, 1846-1851 (1997).
[2] K. Darge, " Voiding urosonography with ultrasound contrast agents for the diagnosis of vesicoureteric reflux in children," Pediatr. Radiol. **38**, 40-53 (2008).
[3] K. L. Stratton, et al., “Implications of ionizing radiation in the pediatric urology patient,” J. Urol. **183**, 2137-2142 (2010).
[4] C. Kim, C. Favazza, and L. V. Wang, “In vivo photoacoustic tomography of chemicals: high-resolution functional and molecular optical imaging at new depths,” Chem. Rev. **110**, 2756-2782 (2010).
[5] C. Kim, K. H. Song, F. Gao, and L. V. Wang, “Sentinel Lymph Nodes and Lymphatic Vessels: Noninvasive Dual-Modality in Vivo Mapping by Using Indocyanine Green in Rats-Volumetric Spectroscopic Photoacoustic Imaging and Planar Fluorescence Imaging,” Radiology **255**, 442-450 (2010).
[6] C. Kim, E. C. Cho, J. Chen, K. H. Song, L. Au, C. Favazza, Q. Zhang, C. M. Cobley, F. Gao, Y. Xia, and L. V. Wang, “In vivo molecular photoacoustic tomography of melanomas targeted by bio-conjugated gold nanocages,” ACSNano **4**, 4559-4564 (2010).
[7] X. Wang, Y. Pang, G. Ku, X. Xie, G. Stoica, and L. V. Wang, “Non-invasive laser-induced photoacoustic tomography for structural and functional imaging of the brain in vivo,” Nat. Biotech. **21**, 803-806 (2003).

[8] S. Jiao, M. Jiang, J. Hu, A. Fawzi, Q. Zhou, K. K. Shung, C. A. Puliafito, and H. F. Zhang, "Photoacoustic ophthalmoscopy for in vivo retinal imaging," Opt. Express **18**, 3967-3972 (2010).
[9] K. Homan, J. Shah, S. Gomez, H. Gensler, A. Karpiouk, L. Brannon-Peppas, and S. Emelianov, "Silver Nanosystems for Photoacoustic Imaging and Image-guided Therapy," J. Biomed. Opt. **15**, 021316 (2010).
[10] E. Todd, C. Kim, M. Pramanik, L. Jankovic, J. Dean, K. Maslov, Z. Guo, M. Pashley, and L. V. Wang, "Noninvasive photoacoustic and ultrasonic imaging of rat sentinel lymph nodes with a clinical ultrasound system," Radiology **256**, 102-110 (2010).
[11] C. Kim, E. Todd, K. Maslov, L. Jankovic, W. J. Arkers, S. Achilefu, J. Margenthaler, M. Pashley, and L. V. Wang, "A hand-held linear array probe for photoacoustic image-guided lymph node biopsy," J. Biomed. Opt. **15**, 146010 (2010).
[12] M. P. Fronheiser, S. A. Ermilov, H. P. Brecht, A. Conjusteau, R. Su, K. Mehta, and A. A. Oraevsky, "Real-time optoacoustic monitoring and three-dimensional mapping of a human arm vasculature," J. Biomed. Opt. 15, 021305 (2010).
[13] C. Kim, E. Todd, L. Jankovic, M. Pashley, and L. V. Wang, "In Vivo Deeply Penetrating Photoacoustic Imaging with a Modified Clinical Ultrasonic Array," Biomed. Opt. Express **1**, 278-284 (2010).
[14] K. Song, and L. V. Wang, "Deep reflection-mode photoacoustic imaging of biological tissue," J. Biomed. Opt. **12**, 060503 (2007).